Available online at www.sciencedirect.com
ScienceDirect
Journal of Power Sources 165 (2007) 120–124
JOURNAL OF POWER SOURCES
www.elsevier.com/locate/jpowsour

Short communication

Highly active lanthanum doped nickel anode for solid oxide fuel cells directly fuelled with methane

Baofeng Tu [a,b], Yonglai Dong [a], Bin Liu [a,b], Mojie Cheng [a,*]

[a] *Dalian Institute of Chemical Physics, Chinese Academy of Sciences, 457 Zhongshan Road, 116023 Dalian, China*
[b] *Graduate School of Chinese Academy of Sciences, Beijing 100039, China*

Received 24 October 2006; received in revised form 25 November 2006; accepted 27 November 2006
Available online 2 January 2007

Abstract

Lanthanum doped nickel and YSZ composite anode (LaNi–YSZ) exhibited a greatly reduced polarization resistance and high performance for electrochemical oxidation of hydrogen and methane, which resulted from a fine anode structure with a high dispersion of nickel catalyst and a high catalytic activity towards methane.

Keywords: Solid oxide fuel cells; LaNi–YSZ anode; Methane

1. Introduction

Solid oxide fuel cells directly utilizing methane offer a promising way for the conversion of chemical energy into electricity both for mobile and stationary applications. The state-of-art anode catalyst nickel shows good activity towards hydrogen fuel, but unfortunately, suffers from carbon deposition using methane fuel which seriously limits the direct application of a natural gas fuel [1]. Alternative approaches to direct-methane fuel cells, such as fuel cells with a ceria-based anode [2], a copper anode [3], a perovskite anode [4,5], or a catalytic reforming layer of noble catalyst [6], have succeeded in reducing carbon deposition but suffered from either a poor anode activity for methane or a high fabrication cost. High activity and a low fabrication cost anode for methane remains a great challenge for the direct-methane solid oxide fuel cell.

As a widely used catalyst, nickel has been well studied in reforming, oxidation and reduction reactions, and the catalytic properties of Ni can be tailored for a specific reaction using a variety of preparation techniques [7]. Different from the conventional catalysts, the nickel particles in an anode are of micro-size and have a weak interaction with the YSZ electrolyte, which results in a low specific active area and low stability. These drawbacks come partially from high temperature sintering processes of NiO–YSZ and the requirement for nickel particles to interconnect into an electrical conduction network. Intrinsically, the low and unstable electrochemical active surfaces arise from the weak interaction between nickel and YSZ or non-wetting properties of nickel on YSZ surface [8,9]. It has been shown that three-phase boundaries in a Ni–YSZ anode form after a current pass over the electrode [10]. Degradation of the interfaces between nickel catalyst and support easily occurs when polluted with carbon deposition. Thus, the improvement of nickel and YSZ interfacial contact is important for a direct methane fuel cell. Here we report a highly active lanthanum modified nickel anode for a direct methane fuel cell. We demonstrate that La addition to nickel catalyst results in a better catalyst–electrolyte contact and a high dispersion of nickel catalyst.

2. Experimental

The new anode we report here was fabricated from YSZ and lanthanum doped nickel oxide. The lanthanum doped nickel oxide powder (5mol% La_2O_3) was prepared from the decomposition and solid-state reaction of nickel nitrate and lanthanum

* Corresponding author. Tel.: +86 411 84379049; fax: +86 411 84379049.
E-mail address: mjcheng@dicp.ac.cn (M. Cheng).

0378-7753/$ – see front matter © 2006 Elsevier B.V. All rights reserved.
doi:10.1016/j.jpowsour.2006.11.058

nitrate. The anode, which was prepared with the conventional tape-casting method, was 2.5 cm in diameter and 1 mm in thickness. An YSZ thin electrolyte film of 15 μm in thickness and an LSM–YSZ cathode were supported on this substrate through co-sintering. A cell with the Ni–YSZ anode was prepared with the same fabrication process as a reference.

The measurements for the cell performances were performed under atmospheric pressure. The cathode was supplied with oxygen at 40 ml min^{-1} at STP, and the anode was supplied either with the humidified methane fuel (3%H_2O) at 20 ml min^{-1} at STP or with the humidified hydrogen (3%H_2O) fuel at 80 ml min^{-1} at STP. The two-probe electrochemical impedance spectra (EIS) were measured in the frequency range of 100,000 to 0.1 Hz under the open circuit condition. The microstructure and microscopy elemental distribution for the traditional Ni–YSZ anode and LaNi–YSZ anode were analyzed by SEM (FEI, QUANTA 200 FEG)-EDAX (EDAX).

3. Results and discussion

Fig. 1 shows the cell performances of cell voltage and power density versus current density for humidified methane and humidified hydrogen fuels. As compared with the Ni–YSZ anode cell, the power densities both for humidified hydrogen fuel and humidified methane fuel increase on the LaNi–YSZ anode cell. A distinguishing feature for the LaNi–YSZ anode cell is that the performance with humidified methane fuel is as high as that for hydrogen fuel. The maximum power density with humidified methane fuel on the LaNi–YSZ anode cell reached to 0.75 W/cm^2 at 700 °C and 1.54 W/cm^2 at 800 °C, which is about the same as 0.79 W/cm^2 at 700 °C and 1.58 W/cm^2 at 800 °C using hydrogen as fuel. Whereas, the cell with the Ni–YSZ anode gives maximum power densities of only 0.27 W/cm^2 at 700 °C and 0.76 W/cm^2 at 800 °C for humidified methane, which are much lower than 0.63 W/cm^2 at 700 °C and 1.39 W/cm^2 at 800 °C using hydrogen as fuel.

The high performance of the LaNi–YSZ anode versus the Ni–YSZ anode is further indicated by the impedance spectra (Fig. 2). The polarization resistance in wet H_2 (97%H_2 + 3% H_2O) at 800 °C was reduced from 0.46 Ω cm^2 for the cell with a Ni–YSZ anode to 0.17 Ω cm^2 for the cell with a LaNi–YSZ anode. More specifically, the polarization resistance R_1 from the high frequency arc is significantly reduced from 0.37 Ω cm^2 for the cell with Ni–YSZ anode to 0.08 Ω cm^2 for the cell with a LaNi–YSZ anode. Electrochemical oxidation of hydrogen on a Ni–YSZ anode is mainly controlled by two-electrode processes, which are featured by two arcs in the impedance spectra, one in the low frequency range associated with the dissociation, adsorption or surface diffusion process and the other in the high frequency range associated with the charge transfer polarization [11,12]. Obviously, the high performance of the LaNi–YSZ anode arises from accelerated charge transfer reactions, which may result from enlarged three-phase boundaries or a better catalyst–electrolyte interface.

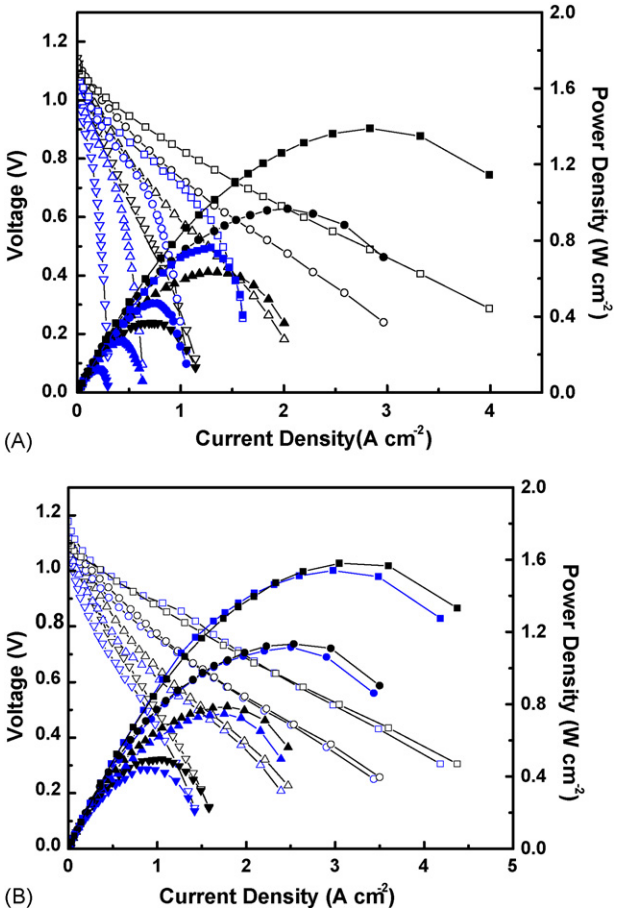

Fig. 1. Cell voltage and power density versus current density for (A) the cell with Ni–YSZ anode and (B) the cell with La Ni–YSZ anode operated on humidified hydrogen (black line and symbol) and humidified methane (blue line and symbol). Squares, 800 °C; circles, 750 °C; triangles, 700 °C; headstand triangles, 650 °C.

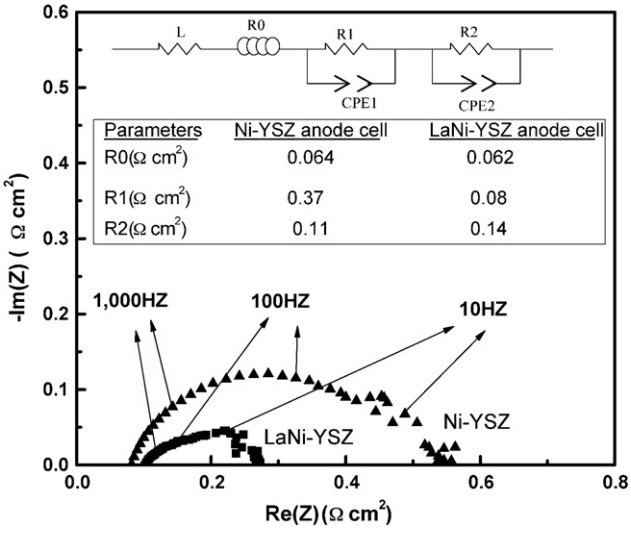

Fig. 2. Impedance spectra of the cell with Ni–YSZ anode and the cell with LaNi–YSZ anode under open circuit potential in 97%H_2 + 3%H_2O at 800 °C. The inlets are the electrochemical impedance model (L, inductor; R_0, ohmic resistance; R_1, resistance of high frequency arc; CPE_1, constant phase element of high frequency arc; R_2, resistance of low frequency arc; CPE_2, constant phase element of low frequency arc) and the corresponding results of the two impedance spectra simulated by CNLS program.

On an SOFC anode, two interpenetrating networks of Ni and YSZ provide for electronic and oxide conductivities respectively, and the interfaces between the nickel and YSZ are responsible for the electrochemical oxidation. The cell performance and polarization resistance are dependent on the anode microstructure. The apparent activation energy of the polarization resistance is high when nickel and YSZ are the point contacts or if the Ni–YSZ cermets are coarse, while it is low for anodes with a fine Ni–YSZ structure [13,14]. The SEM images and microscopic elemental distribution maps (Fig. 3) provide some direct information on the micro-structural difference between the LaNi–YSZ anode and the Ni–YSZ anode. In the SEM micrograph of the Ni–YSZ anode, nickel particles and YSZ particles can be easily discriminated, and a loose contact between nickel and YSZ is observed. The LaNi–YSZ anode shows a smaller and uniform particle size distribution. In the LaNi–YSZ anode, all the small particles have similar crystal shape and are attached together. It is difficult to discriminate which are the nickel particles and which are the YSZ particles in the SEM micrograph. The Zr and Ni elemental dis-

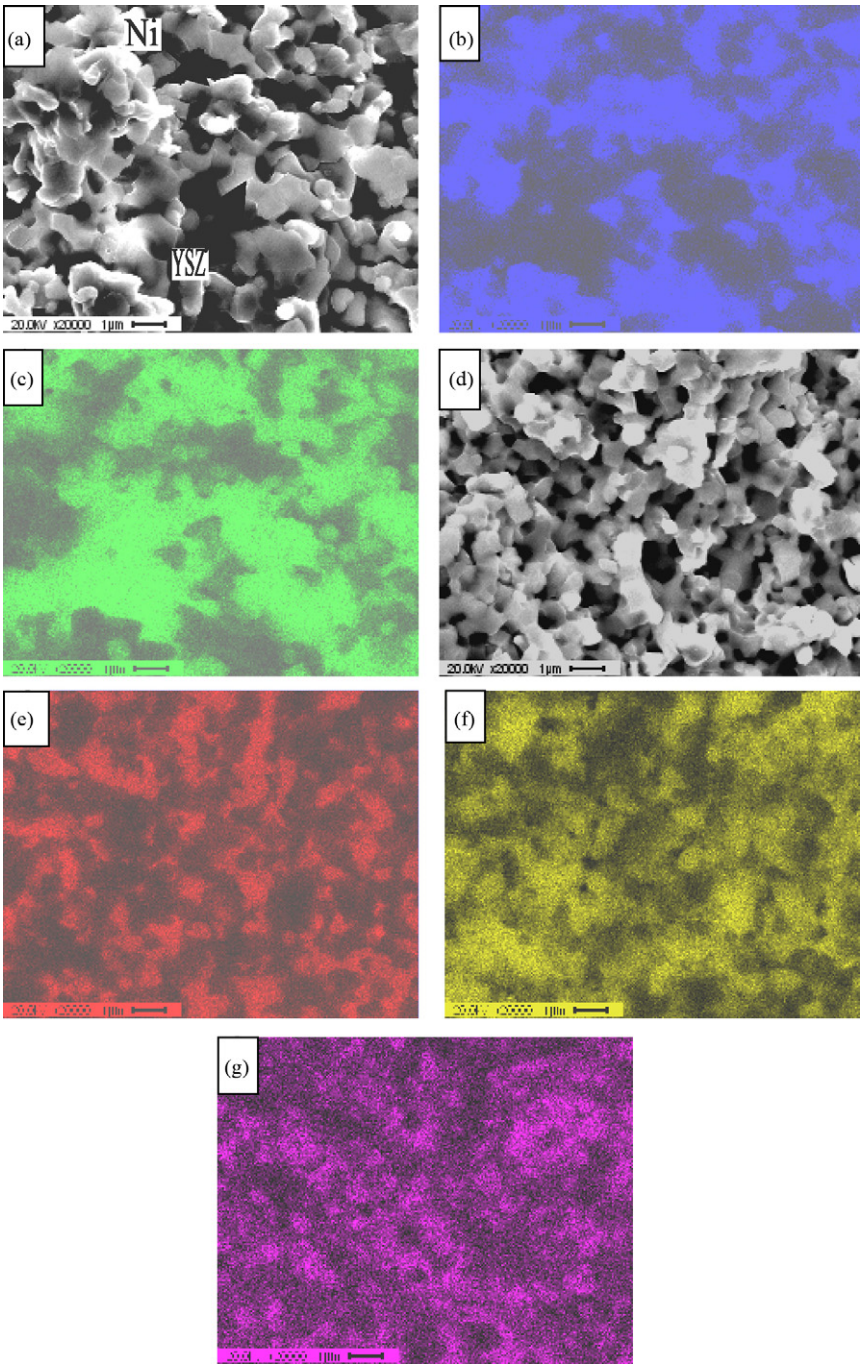

Fig. 3. SEM and EDX elemental images of the (a–c) Ni–YSZ anode and (d–g) LaNi–YSZ anode. (a) SEM, (b) EDX Ni–Ka, (c) EDX Zr–La, (d) SEM, (e) EDX Ni–Ka, (f) EDX Zr–La and (g) EDX La–La.

tribution maps show that nickel and YSZ have a particle size of several micrometers in the Ni–YSZ anode but less than one micrometer in the LaNi–YSZ anode. La has a rather uniform distribution, covering both the nickel and YSZ areas. As indicated by the XRD results, La reacted with nickel and zirconia during preparation.

Electrochemical oxidation of methane on anode is a very complex process including the decomposition of methane, electrochemical oxidation of the products (H_2, CO, C) and reforming of methane by H_2O and CO_2. The rates of the electrochemical reactions in a CH_4–H_2O system are assigned to the rates of the electrochemical oxidation of CH_x, CO, H_2, and C at the interfaces of electrode/electrolyte, among which the oxidation of H_2 is the predominant reaction [15,16]. The oxidation rate of hydrogen can be limited by the H_2 partial pressure, which mainly depends on the activity of methane reforming. Thus, the cell performance for the methane fuel is determined by two processes: methane reforming for hydrogen and the electrochemical oxidation of hydrogen. The reforming processes, including CH_4–CO_2 and CH_4–H_2O reforming, CH_4 decomposition and water–gas-shift reactions, also take place on the anode. So, the electrochemical oxidation of methane is dependent on both electrochemical and non-electrochemical reactions. The La addition greatly hinders the sintering of nickel, and enhances the interaction between the nickel and the YSZ, and thus improves the contact between Ni and YSZ at the metal–ceramic interfaces. On the other hand, La may interact with nickel to increase the activity for reforming methane. The smaller particle size, more uniform distribution, and better interfacial contacts result in higher TPB lengths and so a high activity for reforming methane.

The LaNi–YSZ cell run stably for 10 h on humidified methane at 800 °C, while the Ni–YSZ cell decreased quickly to be very low when the fuel was switched from hydrogen to methane at the same conditions (Fig. 4). For the Ni–YSZ anode, the activity for reforming methane was low, which could not effectively supply hydrogen for the electrochemical reaction, while the rate for electrochemical oxidation of carbon, methane or CO is much lower than hydrogen [15,16]. So, the performance decreases very quickly on a Ni–YSZ anode. Also, the nickel active sites are easily covered and deactivated by deposits of carbon gradually. When most of the active sites are covered by carbon, the rate for methane decomposition is also reduced. It is not a single reaction but a series of reactions which affords the conversion of methane fuel. On the other hand, the coking on the Ni–YSZ anode might result in some cracking of the electrolyte which would make the cell unstable. On the LaNi–YSZ anode cell, high activity for methane reforming supplied enough hydrogen for the electrochemical oxidation process, and the high activity for electrochemical oxidation of hydrogen produced enough H_2O for methane reforming. Thus, the synergy of these reactions in the reaction network and the high activity of the anode catalyst towards these reactions resulted in a high performance anode for direct methane fuel. Since the conversion of methane on the anode depends on a series of reactions in which the decomposition or reforming of methane is the first step, it is important to investigate the synergy of these reactions and the stability of the new anode.

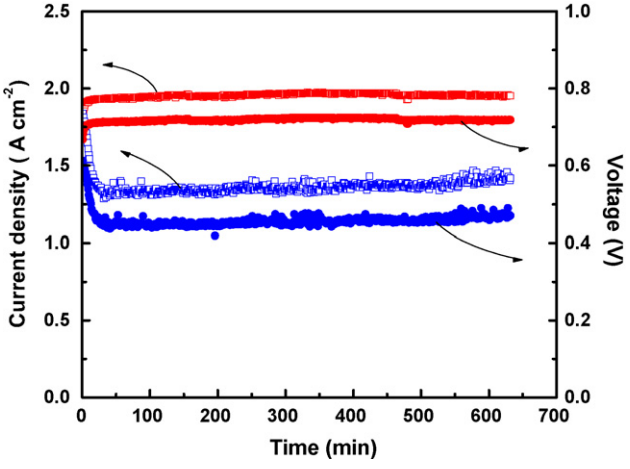

Fig. 4. Stability of the cell operated on humidified methane at 800 °C. (a) the cell with Ni–YSZ anode. Blue open squares, current density; blue filled circuit, voltage; (b) the cell with LaNi–YSZ anode. Red open squares, current density; red filled circuit, voltage. (For interpretation of the references to colour in this figure legend, the reader is referred to the web version of the article.)

4. Conclusions

The present study demonstrates that high power densities and a high power density ratio for methane to hydrogen can be achieved through the modification of the nickel catalyst with La. La addition to the nickel catalyst reduced the polarization resistance and increased the activity for electrochemical oxidation of hydrogen and methane, by hindering the sintering of nickel and YSZ.

Acknowledgments

The authors gratefully acknowledge financial supports from the Ministry of Science and Technology of China (Grant nos. 2004CB719506 and 2005CB221404).

References

[1] A. Atkinson, S. Barnett, R.J. Gorte, J.T.S. Irvine, A.J. Mcevoy, M. Mogensen, S.C. Singhal, J. Vohs, Nat. Mater. 3 (2004) 17–27.
[2] E.P. Murray, T. Tasai, S.A. Barnett, Nature 400 (1999) 649–651.
[3] S. Park, J.M. Vohs, R.J. Gorte, Nature 404 (2000) 265–267.
[4] J.C. Ruiz-Morales, J. Canales-Vazquez, C. Savaniu, D. Marrero-Lopez, W. Zhou, J.T.S. Irvine, Nature 439 (2006) 568–571.
[5] S. Tao, J.T.S. Irvine, Nat. Mater. 2 (2003) 320–323.
[6] Z. Zhan, Y. Lin, M. Pillai, I. Kim, S.A. Barnett, J. Power Sources 161 (2006) 460–465.
[7] Z. Cheng, Q. Wu, J. Li, Q. Zhu, Catal. Today 30 (1996) 147–155.
[8] A. Tsoga, A. Naoumidis, P. Nikolopoulos, Acta Mater. 44 (1996) 3679–3692.
[9] X. Mantzouris, N. Zouvelou, D. Skarmoutsos, P. Nikolopoulos, J. Mater. Sci. 40 (2005) 2471–2475.
[10] A. Aronin, G. Abrosimova, S. Bredikhin, K. Matsuda, K. Maeda, J. Am. Ceram. Soc. 88 (5) (2005) 1180–1185.

[11] S.P. Jiang, S.P.S. Badwal, Solid State Ionics 123 (1999) 209–224.
[12] S.P. Jiang, S.P.S. Badwal, J. Electrochem. Soc. 144 (1997) 3777–3784.
[13] M. Mogensen, S. Skaarup, Solid State Ionics 86–88 (1996) 1151–1160.
[14] M. Brown, S. Primdahl, M. Mogenson, J. Electrochem. Soc. 147 (2) (2000) 475–485.
[15] S. Onuma, A. Kaimai, K. Kawamura, Y. Nigara, T. Kawada, J. Mizusaki, H. Inaba, H. Tagawa, J. Electrochem. Soc. 145 (1998) 920–925.
[16] S. Onuma, A. Kaimai, K. Kawamura, Y. Nigara, T. Kawada, J. Mizusaki, H. Inaba, H. Tagawa, J. Electrochem. Soc. 145 (1998) 3117–3122.